Research Square

Preprints are preliminary reports that have not undergone peer review.
They should not be considered conclusive, used to inform clinical practice,
or referenced by the media as validated information.

3D spheroid models to study tumor colonizing anaerobic bacteria: a bridge from in vitro to in vivo

Jella van de Laak

g.vandelaak@maastrichtuniversity.nl

Maastricht University

Alexandra Mowday

Maastricht University

Yanchao Zhang

Maastricht University

Merve Yildiz

Maastricht University

Ludwig J. Dubois

Maastricht University

Jan Theys

Maastricht University

Research Article

Keywords: Clostridium, spheroids, cancer, CDEPT, the 3R's concept

Posted Date: August 24th, 2026

DOI: https://doi.org/10.21203/rs.3.rs-10551888/v1

License: This work is licensed under a Creative Commons Attribution 4.0 International License.
Read Full License

Additional Declarations: No competing interests reported.

Abstract

Background

Most solid cancers contain areas of necrosis, associated with poor prognosis. This necrotic environment can be exploited by anaerobic bacteria, which selectively colonize tumor necrosis, thereby eliciting anti-cancer effects. Genetic tools “arming” these bacteria with therapeutic genes resulted in the development of a wealth of therapeutic strains. It is essential to validate these strains in robust systems prior to *in vivo* studies. The aim of this study was to develop a 3D *in vitro* model mimicking tumor necrosis, providing an *in vitro* tool to study *Clostridium sporogenes* colonization, antibiotic sensitivity, and therapeutic efficacy.

Methods

Spheroids were generated from Lewis Lung Carcinoma (LLC), CT26, and HCT116 cancer cells and development of necrotic areas was assessed. After *Clostridium sporogenes* spore addition, intra-spheroid colonization was determined. Next, spheroids were utilized to test antibiotics for their ability to clear intra-spheroid colonization and to assess the ability to reproduce *in vivo* therapeutic efficacy of Clostridium-Directed Enzymatic Prodrug Therapy (CDEPT).

Results

LLC spheroids had a growth rate ~ 4-fold higher compared to CT26. Nevertheless, both spheroid models developed necrosis overtime. Spore addition resulted in colonization in both models up to ~$3x10^5$ and ~$3x10^6$ colony forming units (CFU)/spheroid for LLC and CT26, respectively. When utilizing colonized spheroids for studying antibiotic sensitivity, augmentin and vancomycin decreased CFU/spheroid to undetectable levels, whereas tigecycline only temporarily inhibited bacterial growth. In context of CDEPT, CT26 spheroids showed significant spheroid growth inhibition ($P \leq 0.0001$) when treated with both *C. sporogenes-NT-NmeNTR* and prodrug PR-104A, compared to monotherapy. A similar trend, but no significant effect, was observed when reperforming this experiment in HCT116 spheroids.

Conclusion

LLC, CT26, and HCT116 spheroid can be colonized by *C. sporogenes* and used to study colonization-specific aspects *in vitro*. We observed that spheroids can be used for studying antibiotic sensitivity and distinguishing between bacteriostatic and bactericidal effects. Furthermore, we observed that therapeutic effects of CDEPT on spheroids are in line with previous *in vivo* results. These results highlight the potential of 3D *in vitro* models, serving as an important intermediate validation step before embarking *in vivo* studies.

Introduction

Solid tumors are characterized by rapid cell proliferation, often with a disorganized vasculature and outgrowth blood supply. This abnormal vascularity, causing nutrient and oxygen deprivation, can lead to

hypoxic and eventually anoxic intratumoral areas and tumor necrosis. Necrosis is a common feature for most solid tumor types [1] with prevalence numbers ranging from 28% in renal cell carcinoma to 95.9% in colorectal cancer [2, 3]. For all cancer types, tumor necrosis is a marker of poor prognosis and an independent predictor for overall survival [4–8].

Interestingly, tumor necrosis is specific for neoplasms, which has led to the development of tumor-targeted therapies based on this characteristic, including bacterial-based anti-cancer treatments. This decades-old concept relies on intratumoral colonization with anaerobic bacteria, thereby evoking anti-tumor effects, through modulation of the immunological tumor microenvironment, amongst others [9]. A variety of anaerobic bacterial species have been studied as anti-cancer therapies, both *in vitro* and *in vivo*, including the Bifidobacterium and Clostridium species. *Bifidobacterium longum* selectively proliferated in both tumor-bearing mice and rats after systemic administration and *B. adolescentis* was shown to induce apoptosis in tumor-bearing mice [10–12]. Both *in vivo* murine and dog studies with *Clostridium novyi-NT* (nontoxic) [13] showed anti-cancer effects through tumor cell lysis and host immune system activation [14, 15]. Later on, Phase I clinical trials with the *C. Novyi-NT* strain observed germination in the tumor upon a single dose intratumoral bacterial spore injection, resulting in cancer cell lysis and increased infiltration of T and myeloid cells [16, 17].

As an alternative for *C. novyi-NT*, the non-pathogenic *C. sporogenes* has been exploited for its anti-cancer effects. Systemic spore injection with this bacterium resulted in intra-tumoral colonization in tumor-bearing mice and rats [18, 19]. Furthermore, tools to genetically modify *C. sporogenes* have been developed [20, 21]. Application of this methodology allowed the construction of *C. sporogenes-NT* by deleting a gene with high sequence similarity to the Streptolysin S (SLS) operon [22]. Furthermore, modification tools allowed the development of a wide variety of genetically engineered strains capable of expressing and secreting therapeutic proteins. Initially, plasmids carrying a gene encoding for a prodrug-converting enzyme were inserted into *C. sporogenes*. This concept of Clostridium-Directed Enzyme Prodrug Therapy (CDEPT) demonstrated, upon intravenous spore injection, intratumoral colonization, prodrug activation, and improved overall survival *in vivo* [23, 24]. *In vivo* intravenous spore injection of *C. sporogenes-NT* in tumor-bearing animals resulted in high levels of intra-tumoral vegetative cells [22]. Additionally, plasmid insertion with an interleukin (IL)-2 encoding gene resulted in successful secretion of IL-2 by *C. sporogenes-NT*. To increase stability of inserted genes, tools to allow chromosomal integration, such as CRISPR-Cas, were then exploited. Chromosomal integration of various genes, both immunotherapeutic and prodrug converting enzymes, in *C. sporogenes-NT* resulted in successful gene expression and protein/drug secretion [21].

With the emergence of powerful genetic engineering tools that make the development of new therapeutic bacterial strains much easier and faster, there is an urgent need for robust *in vitro* validation models to identify the most promising bacterial strains for further therapeutic development. The key factor required for this model is tumor necrosis, as this is essential to enable effective intratumoral colonization of anaerobic bacteria. However, traditional 2D cellular monolayers fall short in mimicking this necrotic environment. Furthermore, the use of animal models is increasingly constrained by ethical

considerations and regulatory pressure to replace, reduce, and refine animal experimentation. 3D spheroids are dynamic *in vitro* models that better replicate the complexity of the tumor microenvironment by developing hypoxia [25]. These spheroids have already been proven invaluable for studying bacterial colonization for species such as *Salmonella typhimurium*, *Listeria monocytogenes*, *Proteus mirabilis* and *Escherichia coli* [26–29]. While C*lostridium* has also been observed to colonize spheroids [29], the role of necrosis and its interplay with colonization and bacterial effects remain largely unexplored, we present an innovative platform to fill this gap: necrotic spheroid models developed from a range of murine and human cell lines, specifically tailored to study anaerobic bacterial colonization, antibiotic sensitivity, and anti-cancer therapeutic potential. Notably, this spheroid system not only allows for detailed *in vitro* exploration but also provided a tool for studying therapeutic effects with results in line with previous *in vivo* results, marking a significant step toward bridging the gap from *in vitro* to *in vivo* research applications.

Materials and Methods

Spheroid culture

Human HCT116, murine Lewis lung carcinoma (LLC) and CT26 cells were cultured in DMEM or RPMI (Sigma-Aldrich D6429) supplemented with 8% Fetal Bovine Serum (FBS, Bodinco, 5010) at 37°C and 5% CO_2. For spheroid generation, cells were seeded in a 96-well Clear Round Bottom Ultra Low Attachment Microplate (Corning, 7007) in concentrations of 200 cells/well for LLC or 1000 cells/well for CT26 and HCT116. Plates were spun down for 10 minutes at 1000 rpm and left in a 5% CO_2 incubator at 37°C for at least three days to allow formation of a stable spheroid. Spheroid development was monitored using an Olympus-IX81 microscope and spheroid volume was analyzed using MATLAB R2019a software. Final spheroid volume was normalized to spheroid volume on day 5 (start treatment).

Quantification of spheroid necrotic fraction

Spheroid necrosis was visualized using hematoxylin and eosin (H&E) staining. For fixation, spheroids were transferred to 4% formalin (Merck, HT5011) and left overnight. The next day, spheroids were embedded in Epredia™ HistoGel™ Specimen Processing Gel (Thermo Fisher, 12006679), placed in a cassette, and stored in 4% formalin until further processing. After paraffin embedding, spheroids were sectioned using a Leica RM 2255 Microtome at 7uM and incubated overnight at 37°C. Afterwards, sections were deparaffinized using xylene (2x 5 min) (VWR, 28973363) and rehydrated using a graded ethanol series (Supelco, 1.00983) and finally 5 min in milliQ. Next, sections were stained with hematoxylin (VWR, BAKR3870.1000) for 7 min, washed with tap water for 10 min, and stained with eosin (Carl Roth, 229C.2) for 3 min. After staining, cells were dehydrated using an increasing range of ethanol (50%-100%) and xylene for 5 min. Sections were mounted using DPX mounting medium (Sigma-Aldrich, 06522). Slides were scanned using a Precipoint M8 microscope (20x magnification) and analyzed using Viewpoint software and ImageJ, whereby the necrotic area was calculated as a percentage from total spheroid area. In addition, spheroids (n = 20) were pooled and single cells were obtained using trypsin.

Cells were washed once in FACS buffer (0.1% FBS in 1x PBS), diluted to appropriate concentrations (0.25-1.0 x10^7 cells/mL), and stained with propidium iodide (PI, Biolegend, 640914, diluted 1:500). Samples were flushed through a Falcon 5 ml polystyrene cell-strainer-capped tube (VWR 734-0001) prior to measurement. Cells positive for PI were considered as necrotic. Samples were analyzed using BD Bioscience FacsCanto II Flow Cytometer and corresponding software.

Bacterial cultures

C. sporogenes-WT (NCIMB 10696, wildtype), *C. sporogenes-NT*, *C. sporogenes-unaG*, and *C. sporogenes-NT-NmeNTR* were used during the experiments. Methods regarding generation of the NT strain, plasmid-based insertion (unaG gene) and chromosomal integration (NmeNTR gene) are described elsewhere [20, 22, 30]. Bacterial liquid cultures were maintained in Peptone (20 mg/mL, Merck, 18332), Yeast (15 mg/mL, Merck, 71279), and sodium Thioglycolate (1 mg/mL, Merck, T0632) media (PYT). For bacterial solid plate cultures, PYT medium was supplemented with 15 mg/mL Oxoid Agar Technical (Agar No. 2, Thermo Fisher, LP0012B). Growth of *C. sporogenes* strains was carried out in an anaerobic cabinet (model MG1000 Mark II, Don Whitley Scientific Ltd.; 80% N_2, 10% CO_2, 10% H_2) at 37°C. *C. sporogenes-unaG* was generated by inserting the unaG gene (an anaerobic fluorescent gene) and a Pfdx promoter into the pGG2121 plasmid [20]. To maintain introduced pGG2121 plasmids, PYT media was supplemented with chloramphenicol (25 µg/ml for solid media and 12.5 µg/ml for liquid media, Merck, C0378). To induce intra-spheroid colonization, *C. sporogenes* spores were added (1000 spores/spheroid) at day 5 post spheroid seeding.

Sporulation, spore purification, and dilution plating assay

To induce sporulation, 100uL overnight liquid culture was streaked on PYT agar plates and grown over 5 days in an anoxic chamber. After incubation, spores and vegetative bacteria were removed from the plates using cell scrapers, resuspended in PBS, heat treated for 20 min at 80°C, and pelleted by centrifugation (10 min at 10000g). Spores were separated from vegetative bacteria using a density gradient [31] by resuspending the pellet in 2.5 mL 20% Histodenz (Merck, D2158). Next, 250 µL of this suspension was added to 750 µL 50% Histodenz and centrifuged at 20000g, 4°C for 60 min. Vegetative bacteria were present at the junction of the two layers, while the spores were pelleted at the bottom of the lower layer. Supernatant (both layers) was removed, and spores were washed 3 times with sterile water, resuspended in PBS and stored at 4°C until further use. Spore stock concentration was determined using the dilution plating assay. Spore stock was serially diluted, spotted (20 µL per spot) on PYT agar plates, and left overnight in an anoxic environment to allow bacterial growth. Next day, colonies were counted and colony forming unit (CFU)/mL was calculated based on the dilution factor.

Detection and quantification of intra-spheroid colonization

Spheroids were individually washed with PBS and trypsinized until single cells were obtained. Trypsin was inhibited using cell culture medium and CFU/spheroid was determined using the abovementioned dilution plating assay. Additionally, bacterial presence and location were assessed on paraffin embedded

sections using Gram-Twort staining. After rehydration, sections were first stained with crystal violet (Merck, V5265) for 10s, quickly washed in demineralized water and incubated with Gram's iodine solution (Merck, 90107-250ML-F) for 30s. Next, sections were washed in demineralized water and decolorized in 90% ethanol. Counterstaining was performed for 2 min using a mixture of 30% fast green (0.2% solution in 95% ethanol, Merck, F7258) and 3.3% neutral red (0.2% solution in 95% ethanol, Merck, C.I. 50040) in demineralized water. Sections were dried, mounted using DPX mounting medium, and visualized using a Nikon Eclipse E800 microscope and ACT-1 software.

CDEPT approach in spheroids

The CDEPT approach was performed by adding either *C. sporogenes-NT* or *C. sporogenes-NT-NmeNTR* spores to the spheroid media at day 5, PR-104A (MCE, HY-14572) or DMSO in various concentrations at day 7, washing the spheroids at day 8 to remove the prodrug, and monitoring the therapeutic effects until day 15. Spheroid volume of each treatment arm within the individual PR-104A concentration groups was normalized to the corresponding DMSO control.

Statistical analysis

All data presented in this manuscript represents the results of at least three biological replicates. Statistical evaluations were performed with GraphPad Prism 8.0.2 software (San Diego, CA, United States). For the analysis of spheroid growth, and to compare spheroid volume of LLC and CT26 of each timepoint, normality was assessed and an unpaired *t*-test was used. Normal distribution has been assessed using the Shapiro-Wilk test and when $P > 0.05$, data was assumed to be normal distributed. To compare spheroid growth inhibition between different treatment groups, the *C. sporogenes-NT-NmeNTR* spheroid volume was compared to the other treatment groups. Each PR-104A concentration dataset was analyzed individually and data was analyzed using one-way ANOVA with Dunnett's post-test. P-values were considered as follows: $P > 0.05$ (not significant, ns), $P < 0.05$ (*), $P < 0.01$ (**), $P < 0.001$ (***), $P < 0.0001$ (****). To assess synergism between *C. sporogenes-NT-NmeNTR* and PR-104A treatment, the Bliss independence score has been applied, whereby a score > 10 is considered as a synergistic effect [32].

Results

LLC and CT26 spheroids develop necrosis

Spheroid growth and the development of necrosis was followed from 5 days post-seeding CT26 and LLC spheroids. LLC spheroids (doubling time: 0.6 days) grew faster compared to CT26 spheroids (doubling time: 2.3 days). Consequently, the LLC spheroids reached a volume approximately 10-fold ($P < 0.0001$) larger on day 12 compared to the CT26 spheroids (Fig. 1a and b). Development of spheroid necrosis from day 6 onwards was confirmed by H&E staining in both spheroid models and the percentage of

necrotic area increased overtime (Fig. 1c and d). Flowcytometry confirmed necrosis development in CT26 and LLC spheroids on day 6 and 8 post-seeding (Fig. 1e).

C. sporogenes germinates and colonizes LLC and CT26 spheroids

To assess germination and colonization properties of *C. sporogenes* in both spheroid models, *C. sporogenes-WT* spores were added to the spheroid culture medium at day 5 post spheroid seeding. Afterwards, spheroid growth and colonization were monitored daily until day 12 (Fig. 2a). For LLC, upon adding *C. sporogenes-WT* spores, the shape of the spheroids started to change on day 8 until the spheroids ultimately disintegrated by day 10, compared to untreated controls (figure c). CT26 spheroid morphology was not affected after incubation with *C. sporogenes-WT* spores until day 12. Intra-spheroid colonization in the LLC model peaked at day 7 and decreased until a point where no more bacteria could be detected, corresponding with the time point of spheroid disintegration (Fig. 2b and 2c). For CT26, intra-spheroid colonization increased until day 10 and stabilized at later time points. Additionally, we investigated the possibility to non-invasively monitor intra-spheroid colonization using the fluorescent *C. sporogenes-unaG.* Presence of fluorescent bacteria could be detected in both LLC and CT26 spheroids on day 7 and 9 respectively while fluorescent signals were absent in spheroid treated with *C. sporogenes-WT* (Fig. 2d) and confirmed successful intra-spheroid bacterial germination. Likewise, Gram-Twort staining confirmed the presence of gram-positive, i.e. red/purple stained, vegetative bacteria within the necrotic areas of both spheroid models (Fig. 3), while bacteria are absent in the viable spheroid area.

Intra-spheroid spheroid colonization is reversible with antibiotic treatment

Antibiotic sensitivity of *C. sporogenes* is an important safety mechanism for our bacterial-based anti-cancer therapy as this allows removal of the bacteria from the patient's tumor at any time. We used our optimized spheroid model, and the disintegration effect of the bacteria to LLC spheroids, to study antibiotic clearance of intra-spheroid colonization by *C. sporogenes*. First, we determined the minimal inhibitory concentration (MIC) for *C. sporogenes* against a panel of antibiotics on agar plates (supplementary Fig. 1). Vancomycin, augmentin, metronidazole and tigecycline were selected for subsequent spheroid testing based on their capacity to inhibit bacterial growth on plates, their variety of mechanisms of action, and their utility in clinical settings. As antibiotic sensitivity testing on agar plates does not distinguish between inhibition of bacterial growth (bacteriostatic properties) or actual killing of bacteria (bactericidal properties), spheroids were then used to test antibiotic clearance of our bacteria, for which bactericidal antibiotics are required. After LLC spheroid generation, *C. sporogenes-NT* spores were added on day 5, colonization on day 6 was confirmed (Fig. 4c-f, day 6), antibiotics were added using the previously determined MIC and a 10-fold higher concentration (MICx10), and intra-spheroid colonization was monitored until day 12 (Fig. 4a). Spheroids treated with spores and vehicle (DMSO) disintegrated with time compared to vehicle treatment only (Fig. 4b), indicating bacterial colonization as previously observed.

Tigecycline MIC was not effective as bacterial numbers increased overtime, resulting in spheroid disintegration. In contrast, MICx10 decreased bacterial growth until day 9. At later time-points, bacterial growth increased again until spheroid disintegration was observed (Fig. 4c). Metronidazole fully cleared bacterial colonization by day 8 (Fig. 4d). Unexpectedly, spheroids treated with MICx10 metronidazole disintegrated despite the low, or even undetectable, CFU/spheroid (Fig. 4d). Augmentin and vancomycin were both able to clear intra-spheroid colonization. Augmentin MICx10 fully inhibited bacterial growth after day 9 whereas MIC only partially within 12 days (Fig. 4e), keeping spheroids intact. Vancomycin MIC (day 10) and MICx10 (day 9) were both effective for clearing intra-spheroid colonization (Fig. 4f), with fully restored spheroid stability.

Spheroids as useful tools to assess therapeutic efficacy of genetically modified C. sporogenes in a CDEPT approach

To bridge the gap from *in vitro* to *in vivo*, we investigated whether spheroids can be used to evaluate the therapeutic response upon colonization with genetically engineered *C. sporogenes* in a CDEPT approach, thereby confirming that spheroid can be utilized to test therapeutic efficacy *in vitro* [23, 24]. We added *C. sporogenes-NT-NmeNTR*, a *C. sporogenes* strain expressing the NmeNTR enzyme which is able to convert the prodrug PR-104A into its toxic derivative [30], to both CT26 (Fig. 5) and HCT116 (Fig. 6) spheroids. After adding the prodrug, we followed spheroid growth until day 15 post seeding (Fig. 5a).

A significantly smaller volume was observed for CT26 spheroids treated with *C. sporogenes-NT-NmeNTR* and PR-104A, compared to other treatment groups, for all concentrations of PR-104A (Fig. 5b-c, $P < 0.001$). The effects of treatment with *C. sporogenes-NT-NmeNTR* and PR-104A resulted in Bliss scores of 37, 29, and 32 for 10 µM, 20 µM, and 30 µM PR-104A treatment groups, respectively, indicating synergism. Furthermore, CT26 spheroids likewise show signs of disintegration when treated with bacteria only on day 15 (Fig. 5b). As the CDEPT approach has been tested *in vivo* in HCT116 tumor-bearing animals before [23], we validated our findings in HCT116 spheroids. After verification of intra-spheroid colonization in HCT116 spheroids 24 and 72h after spore addition on day 5 (Fig. 6a) and following the effects of intra-spheroid colonization on spheroid development (Fig. 6b), a similar experiment was executed. HCT116 spheroids were smaller compared to CT26 spheroids and showed signs of disintegration upon bacterial colonization (Fig. 6d). Spheroid growth inhibition was observed upon combination treatment of *C. sporogenes-NT-NmeNTR* and PR-104A compared to vehicle treatment ($P < 0.001$). However, while lower spheroid volumes were observed, no significant differences were found in spheroids treated with *C. sporogenes-NT-NmeNTR* and PR-104A compared to monotherapy treatment groups (Fig. 6c and 6d).

Discussion

The use of spheroids in cancer research has been extensively investigated over the past decades, mainly since this 3D model is able to mimic tumor hypoxia and necrosis, characteristics of the tumor microenvironment [33–35]. Also in the field of bacterial-based anti-cancer therapies, the use of

spheroids has been described, as exemplified by Harimoto et al who developed a method to co-culture facultative anaerobe Salmonella bacteria with cancer spheroids [26]. In the current study, we have demonstrated the utility of 3D *in vitro* spheroid models to build a bridge between *in vitro* and *in vivo* studies in the context of obligate anaerobe *C. sporogenes*-based anti-cancer therapy. We have shown that necrotic spheroid models (both murine and human) allow intra-spheroid colonization with different *C. sporogenes* strains, in line with previously shown *in vivo* intra-tumoral colonization [22]. Additionally, we have demonstrated that this spheroid model can be used for the *in vitro* validation of bacterial characteristics such as colonization, antibiotic sensitivity, and therapeutic efficacy, thereby providing a strategy for selection of potential successful strains prior to embarking *in vivo* studies.

In contrast to the work of Harimoto et al, we focused on the development of necrotic spheroids as these provide a niche for obligate anaerobic bacteria to thrive in. Our findings showed intra-spheroid colonization for all spheroid models and vegetative bacteria were present specifically in the anoxic areas, recapitulating the observations of Osswald et al [29]. We have confirmed the presence of bacteria using bacterial assays and localized the bacteria using Gram staining and live imaging of fluorescent *C. sporogenes-unaG*. We observed that necrotic lesions, and therefore bacterial colonization, is not restricted to the core of the spheroid (as depicted in Fig. 2d and 3). Osswald et al generated spheroids by co-seeding spores and cells to establish intra-spheroid colonization, while we focused on adding spores when necrosis was present (5 days post-seeding) and investigated the effects of intra-spheroid colonization on spheroid development. In contrast to Osswald et al, we observed an impairment in spheroid growth when treated with spores, resulting in disintegration over time for the LLC model. This effect may be attributed to extracellular matrix (ECM) breakdown, as described by Bhave et al, where proteins from heat-inactivated *C. sporogenes* resulted in reduced spheroid growth due to break-down the ECM [36]. Nevertheless, vegetative bacteria were detected in both LLC and CT26 models thereby providing evidence that these spheroids provide an *in vitro* tool for mimicking intra-tumoral colonization.

Confirmation of the presence of intra-spheroid colonization allowed us to use the spheroid model for testing various colonization specific aspects, such as antibiotic sensitivity, i.e. to examine the ability of various antibiotics to clear intra-spheroid colonization. Tigecycline is an antibiotic that exhibits both bactericidal and bacteriostatic properties [37, 38]. In our spheroid models, tigecycline showed bacteriostatic rather than bactericidal properties, as intra-spheroid colonization was restored after several days. Clinical relevance of testing *in vitro* antibiotic sensitivity has been questioned before as it is difficult to correlate an *in vitro* setting to *in vivo* effectiveness of the antibiotics [39]. There are several *in vivo* factors that might influence the effectiveness of the antibiotics, such as antibiotic clearance by the body. Although the spheroid system cannot mimic *in vivo* antibiotic effectivity, it does allow to differentiate between bacteriostatic and bactericidal antibiotics, which cannot be done using standard MIC assays [40]. To fully eradicate the bacterial treatment from the patient, whenever necessary, antibiotics with bactericidal properties are preferred in our studies, such as augmentin and vancomycin, which cleared the spheroids from *C. Sporogenes-NT*. Similar results were obtained with metronidazole MIC. Surprisingly, metronidazole MICx10 treatment resulted in full spheroid disintegration. This can be

explained by the fact that metronidazole is a nitroimidazole, a group of selective hypoxia-activated compounds having hypoxia-specific cytotoxic effects on cancer cells [41, 42].

Next to antibiotic sensitivity we aimed to study therapeutic efficacy using our optimized spheroid models. In the field of bacterial-based anti-cancer therapy, spheroids have been exploited to test therapeutic efficacy *in vitro* and both the effects of intra-spheroid colonization and expression of therapeutic genes have been described [27, 36, 43]. As translation towards *in vivo* studies is frequently absent, the question remained whether spheroid models could be used to provide a bridge between *in vitro* and *in vivo* experiments regarding bacterial based anti-cancer therapies. CDEPT, the combination of clostridia expressing a prodrug converting enzyme and prodrug treatment, has previously proven to result in tumor growth delay *in vivo* [23, 24, 44]. Therefore, we investigated if results obtained with our spheroid system were in line with the outcome of *in vivo* experiments and therefore provide a bridge between *in vitro* and *in vivo* experiments. Similar to previous *in vivo* studies [23], the combination of *C. sporogenes-NT-NmeNTR* with the prodrug PR-104A resulted in spheroid growth inhibition in both CT26 and HCT116 spheroids. Dose and model dependency might be attributed to the differences in size and CFU/spheroid between CT26 and HCT116 spheroids. Additionally, the metabolism of PR-104A differs among human (HCT116) and murine (CT26) cells [45]. Overall, our spheroid models confirm the previously found *in vivo* results showing the effective combination of *C. sporogenes-NT-NmeNTR* and PR-104A.

There are several limitations to consider within this study. Various cell lines have been utilized to develop spheroids with each cell line having different characteristics regarding cell growth, spheroid formation, hypoxic/anoxic fraction, and bacterial-based disintegration. Spheroid models therefore require cell specific optimization prior to using those as *in vitro* models. Spheroid volume was measured using microscopic imaging and spheroid volume quantification software. Flow cytometry analysis would have been an alternative for providing quantitative information regarding the number of cells in spheroids. Furthermore, flow cytometry has been used in this study for providing information regarding the necrotic status of the spheroids. However, flow cytometry analysis bears spheroid model related disadvantages, such as the necessity of pooling spheroids for obtaining the preferred number of cells and the disintegration of spheroids to single cell suspensions prior to flow cytometry. Additionally, in context of our study, long-term necrosis was difficult to detect using flow cytometry due to breakdown of necrotic cellular structure; our results confirm the presence of necrosis as seen on the H&E staining where the necrotic fraction is localized, but do not quantify the actual number of necrotic cells. Similar to antibiotic concentrations, several *in vivo* factors might influence the effectiveness of PR-104A or spore concentration. Hence, the spheroid model cannot mimic testing clinically relevant dosing, and therefore concentrations of spores, antibiotics, and PR-104A should be optimized in *in vivo* settings. However, the spheroid models can be utilized as an *in vitro* selection strategy to refine *in vivo* experiments or as selection model for screening a subset of drugs and narrow the number down for further *in vivo* analysis. An alternative 3D model to spheroids is the use of organoids. Tumor organoids are widely used in context of cancer research and non-tumor organoids are described in co-cultures with microbes [46, 47]. However, to our knowledge, thus far organoids have not been studied in context of anaerobe bacterial-

based anti-cancer therapies. Where spheroids are generated usually from one or two different established cell lines, tumor organoids consist of clusters of tumor-specific cells derived from patients. Hence, tumor organoids can be used for in-depth analysis of several cancer types in a personalized manner [48]. While tumor organoids enable a more detailed and complex reflection of the TME, such models can be challenging to generate, and reproducibility remains questionable [49]. Nevertheless, tumor organoids for *in vitro* validation of anaerobe bacterial based anti-cancer therapy might be a valuable tool for more detailed information.

Conclusion

In this study, spheroids have been optimized and utilized to study bacteria as tumor-targeting therapy, however, other tumor-related aspects could potentially be investigated using spheroid models. For example, the presence of bacteria in tumors, the tumor microbiota, is state-of-the-art research and spheroids are used to investigate the presence and the effect of these intra-tumoral bacteria [28, 50]. Furthermore, spheroid models have been used in a co-culture setting with immune cells [51–53] and these co-culture models might be interesting to use in context of immunotherapeutic-expressing bacteria [22]. Our data demonstrates that spheroid models from both murine and human cell lines can bridge the gap from “simple” *in vitro* studies to complex *in vivo* studies in context of both aerobe [26] and anaerobe (current study) bacterial-based anti-cancer therapies. Spheroid models enable studying colonization specific aspects of the bacteria such as germination, growth, and antibiotic sensitivity. Moreover, this novel tool allows testing therapeutic efficacy and selection of the most efficient bacterial strains to take forward to *in vivo* studies, being a significant step for *in vitro* optimization of bacterial-based anti-cancer strategies in a world where new anti-cancer bacterial strains are developed rapidly.

Abbreviations

CDEPT
Clostridium-Directed Enzyme Prodrug Therapy
CFU
Colony forming units
ECM
Extracellular matrix
H&E
hematoxylin and eosin
IL
Interleukin
LLC
Lewis lung carcinoma
MIC
minimal inhibitory concentration
NT

Nontoxic
PI
propidium iodide
SLS
Streptolysin S

Declarations

Ethics approval and consent to participate

Not applicable

Consent for publication

Not applicable

Funding

This project received funding from KWF grant number 13056 “Exploiting recombinant Clostridium for precise delivery of immunotherapeutic to solid tumors”.

Author Contribution

Experimental design –JL, AM, LJD, JT. Execution of in vitro studies – JL, AM, YZ, MY. Data analysis and discussion – JL, AM, LJD, JT. Manuscript writing – JL, AM, LJD, JT. All authors revised and agreed on the content described in the manuscript.

Acknowledgement

The authors thank Natasja Lieuwes, Rianne Biemans, Pim Ritt, and Sandra Formen for technical support in the laboratory. This project received funding from KWF grant number 13056 “Exploiting recombinant Clostridium for precise delivery of immunotherapeutic to solid tumors”. Figures have been generated using Biorender.

Availability of data and materials

The data analyzed during the current study are available from the corresponding author on reasonable request.

Competing interests

LJD has, outside of the submitted work, shares in the company Convert Pharmaceuticals. JT and LJD have, in context of the submitted work, shares in the company LivingMed Biotech. The other authors declare that the research was conducted in the absence of any commercial or financial relationships that could be construed as potential conflict of interest.

References

1. Richards CH, et al. The prognostic value of histological tumor necrosis in solid organ malignant disease: a systematic review. Future Oncol. 2011;7(10):1223–35.
2. Sengupta S, et al. Histologic coagulative tumor necrosis as a prognostic indicator of renal cell carcinoma aggressiveness. Cancer: Interdisciplinary Int J Am Cancer Soc. 2005;104(3):511–20.
3. Väyrynen SA, et al. Clinical impact and network of determinants of tumour necrosis in colorectal cancer. Br J Cancer. 2016;114(12):1334–42.
4. Hiraoka N, et al. Tumour necrosis is a postoperative prognostic marker for pancreatic cancer patients with a high interobserver reproducibility in histological evaluation. Br J Cancer. 2010;103(7):1057–65.
5. Muz B et al. *The role of hypoxia in cancer progression, angiogenesis, metastasis, and resistance to therapy.* Hypoxia, 2015: pp. 83–92.
6. Beckers C, Pruschy M, Vetrugno I. Tumor hypoxia and radiotherapy: a major driver of resistance even for novel radiotherapy modalities. Seminars in Cancer Biology. Elsevier; 2024.
7. Kopecka J, et al. Hypoxia as a driver of resistance to immunotherapy. Drug Resist Updates. 2021;59:100787.
8. Luo W, Wang Y. Hypoxia mediates tumor malignancy and therapy resistance. Hypoxia Cancer Metastasis, 2019: pp. 1–18.
9. Mowday AM, et al. Tumor-targeting bacteria as immune stimulants–the future of cancer immunotherapy? Crit Rev Microbiol. 2024;50(6):955–70.
10. Wang L, et al. *Roles of bifidobacterium on prevention of experimental colorectal carcinoma and induction of apoptosis.* Zhonghua yu fang yi xue za zhi. [Chinese J Prev Medicine]. 1999;33(6):337–9.
11. Yazawa K, et al. Bifidobacterium longum as a delivery system for gene therapy of chemically induced rat mammary tumors. Breast Cancer Res Treat. 2001;66:165–70.
12. Fujimori M. Genetically engineered bifidobacterium as a drug delivery system for systemic therapy of metastatic breast cancer patients. Breast Cancer. 2006;13(1):27–31.

13. Dang LH et al. *Combination bacteriolytic therapy for the treatment of experimental tumors.* Proceedings of the National Academy of Sciences, 2001. 98(26): pp. 15155–15160.
14. Agrawal N et al. *Bacteriolytic therapy can generate a potent immune response against experimental tumors.* Proceedings of the National Academy of Sciences, 2004. 101(42): pp. 15172–15177.
15. Roberts NJ et al. *Intratumoral injection of Clostridium novyi-NT spores induces antitumor responses.* Science translational medicine, 2014. 6(249): p. 249ra111-249ra111.
16. Janku F, et al. Intratumoral injection of Clostridium novyi-NT spores in patients with treatment-refractory advanced solid tumors. Clin Cancer Res. 2021;27(1):96–106.
17. Nelson BE et al. Phase Ib study of pembrolizumab in combination with intratumoral injection of Clostridium novyi-NT in patients with advanced solid tumors. Clin Cancer Res, 2025.
18. Theys J, et al. Improvement of Clostridium tumour targeting vectors evaluated in rat rhabdomyosarcomas. FEMS Immunol Med Microbiol. 2001;30(1):37–41.
19. Liu S-C, et al. Anticancer efficacy of systemically delivered anaerobic bacteria as gene therapy vectors targeting tumor hypoxia/necrosis. Gene Ther. 2002;9(4):291–6.
20. Zhang Y, et al. Development of a CRISPR-Cas12a system for efficient genome engineering in clostridia. Microbiol Spectr. 2023;11(6):e02459–23.
21. Kubiak AM, et al. Refined control of CRISPR-Cas9 gene editing in Clostridium sporogenes: the creation of recombinant strains for therapeutic applications. Front Immunol. 2023;14:1241632.
22. Kubiak AM, et al. Efficient secretion of murine IL-2 from an attenuated strain of Clostridium sporogenes, a novel delivery vehicle for cancer immunotherapy. Front Microbiol. 2021;12:669488.
23. Mowday AM, et al. Use of an optimised enzyme/prodrug combination for Clostridia directed enzyme prodrug therapy induces a significant growth delay in necrotic tumours. Cancer Gene Ther. 2022;29(2):178–88.
24. Heap JT, et al. Spores of Clostridium engineered for clinical efficacy and safety cause regression and cure of tumors in vivo. Oncotarget. 2014;5(7):1761.
25. Leek R, et al. Methods: using three-dimensional culture (spheroids) as an in vitro model of tumour hypoxia. Tumor Microenvironment: Study Protocols; 2016. pp. 167–96.
26. Harimoto T et al. *Rapid screening of engineered microbial therapies in a 3D multicellular model.* Proceedings of the National Academy of Sciences, 2019. 116(18): pp. 9002–9007.
27. Harimoto T, Deb D, Danino T. A rapid screening platform to coculture bacteria within tumor spheroids. Nat Protoc. 2022;17(10):2216–39.
28. Kasper SH, et al. Colorectal cancer-associated anaerobic bacteria proliferate in tumor spheroids and alter the microenvironment. Sci Rep. 2020;10(1):5321.
29. Osswald A, et al. Three-dimensional tumor spheroids for in vitro analysis of bacteria as gene delivery vectors in tumor therapy. Microb Cell Fact. 2015;14:1–12.
30. Zhang Y, et al. Heterologous gene regulation in clostridia: rationally designed gene regulation for industrial and medical applications. ACS Synth Biol. 2022;11(11):3817–28.

31. Setlow P. Observations on research with spores of Bacillales and Clostridiales species. J Appl Microbiol. 2019;126(2):348–58.
32. Bliss CI. The toxicity of poisons applied jointly 1. Ann Appl Biol. 1939;26(3):585–615.
33. Franko AJ, Sutherland RM. Oxygen diffusion distance and development of necrosis in multicell spheroids. Radiat Res. 1979;79(3):439–53.
34. Talari ACS, et al. Analyzing normal proliferating, hypoxic and necrotic regions of T-47D human breast cancer spheroids using Raman spectroscopy. Appl Spectrosc Rev. 2017;52(10):909–24.
35. Zhu S, et al. Influence of experimental variables on spheroid attributes. Sci Rep. 2025;15(1):9751.
36. Bhave MS, et al. Effect of heat-inactivated Clostridium sporogenes and its conditioned media on 3-dimensional colorectal cancer cell models. Sci Rep. 2015;5(1):15681.
37. Pournaras S, et al. Activity of tigecycline alone and in combination with colistin and meropenem against Klebsiella pneumoniae carbapenemase (KPC)-producing Enterobacteriaceae strains by time–kill assay. Int J Antimicrob Agents. 2011;37(3):244–7.
38. Tessier PR, Nicolau DP. Tigecycline displays in vivo bactericidal activity against extended-spectrum-β-lactamase-producing Enterobacteriaceae after 72-hour exposure period. Antimicrob Agents Chemother. 2013;57(1):640–2.
39. Stratton CW. In vitro susceptibility testing versus in vivo effectiveness. Med Clin North Am. 2006;90(6):1077–88.
40. Pankey GA, Sabath L. Clinical relevance of bacteriostatic versus bactericidal mechanisms of action in the treatment of Gram-positive bacterial infections. Clin Infect Dis. 2004;38(6):864–70.
41. Koike N, et al. 2-Nitroimidazoles induce mitochondrial stress and ferroptosis in glioma stem cells residing in a hypoxic niche. Commun biology. 2020;3(1):450.
42. Ahmadi H et al. Metronidazole Delivery Strategies: Optimizing Cancer Therapy through Novel Approaches for Enhanced Delivery, Cytotoxicity, and Side Effect Reduction. Eur J Med Chem Rep, 2024: p. 100202.
43. Mokrani N et al. *Magnetotactic bacteria penetration into multicellular tumor spheroids for targeted therapy*. in. 2010 *Annual International Conference of the IEEE Engineering in Medicine and Biology*. 2010. IEEE.
44. Theys J, et al. Repeated cycles of Clostridium-directed enzyme prodrug therapy result in sustained antitumour effects in vivo. Br J Cancer. 2006;95(9):1212–9.
45. Gu Y, Atwell GJ, Wilson WR. Metabolism and excretion of the novel bioreductive prodrug PR-104 in mice, rats, dogs, and humans. Drug Metab Dispos. 2010;38(3):498–508.
46. Puschhof J, et al. Intestinal organoid cocultures with microbes. Nat Protoc. 2021;16(10):4633–49.
47. Lv J, et al. Construction of tumor organoids and their application to cancer research and therapy. Theranostics. 2024;14(3):1101.
48. Tong L, et al. Patient-derived organoids in precision cancer medicine. Med. 2024;5(11):1351–77.

49. Živković Z, Opačak-Bernardi T. An Overview on Spheroid and Organoid Models in Applied Studies. Sci. 2025;7(1):27.
50. Yeung YWS, et al. Bacterial Iron Siderophore Drives Tumor Survival and Ferroptosis Resistance in a Biofilm-Tumor Spheroid Coculture Model. Adv Sci. 2024;11(39):2404467.
51. Al-Hity G, et al. An integrated framework for quantifying immune-tumour interactions in a 3D co-culture model. Commun Biology. 2021;4(1):781.
52. Courau T, et al. Cocultures of human colorectal tumor spheroids with immune cells reveal the therapeutic potential of MICA/B and NKG2A targeting for cancer treatment. J Immunother Cancer. 2019;7:1–14.
53. Tevis KM, et al. Mimicking the tumor microenvironment to regulate macrophage phenotype and assessing chemotherapeutic efficacy in embedded cancer cell/macrophage spheroid models. Acta Biomater. 2017;50:271–9.

Figures

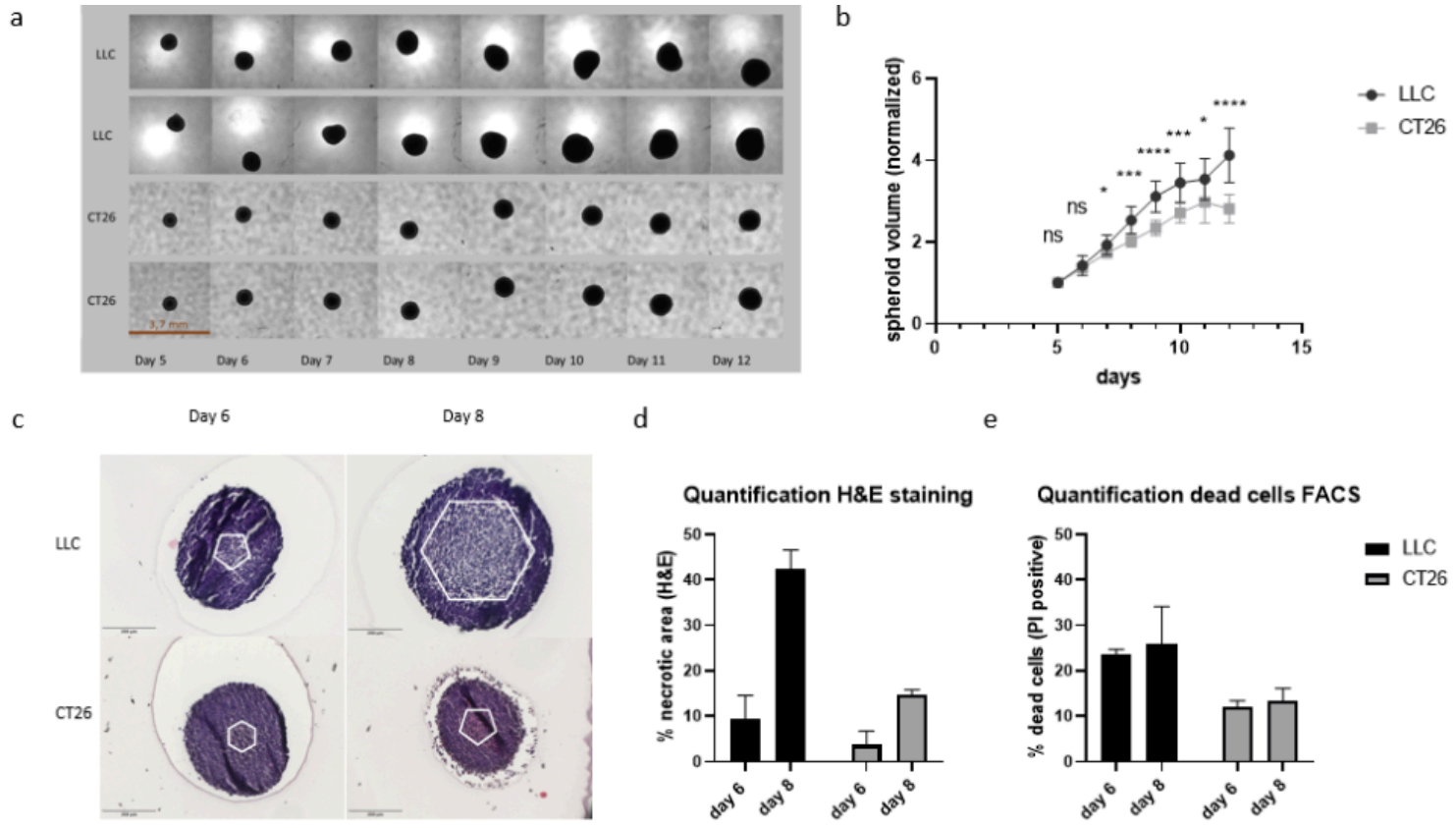


Figure 1

LLC and CT26 spheroids develop a necrotic core over time*. a: Representative images (4x magnification) of LLC and CT26 spheroids overtime. b: Volume of LLC (n=12) and CT26 (n=9) spheroids over time. Representative H&E staining (necrotic area indicated with white delineation) (c) and quantification of %*

necrotic area (d) of LLC and CT26 spheroids on day 6 and day 8. e: Quantification of PI positive cells in LLC and CT26 spheroids (N=3 pooled samples per time point).

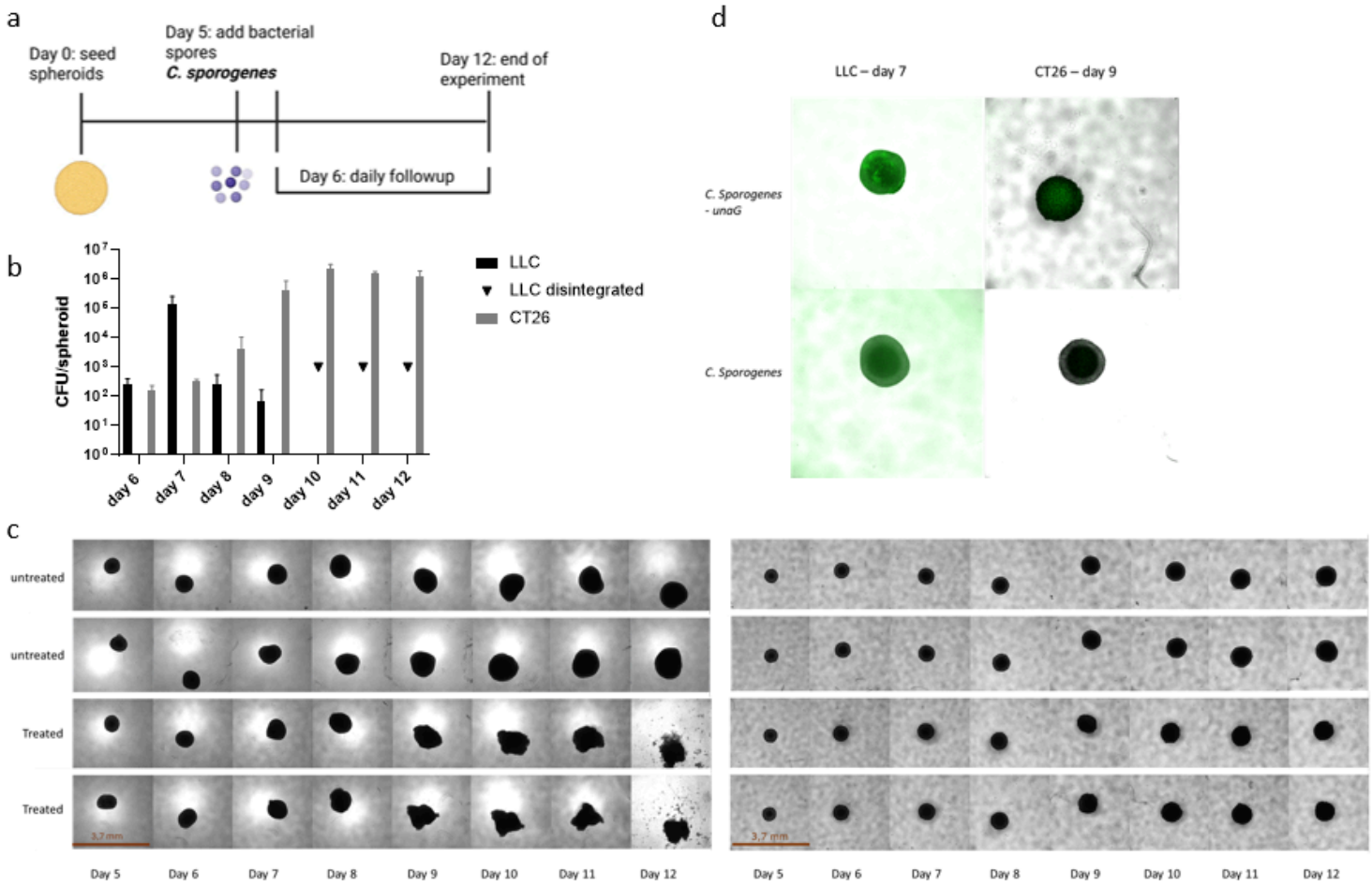


Figure 2

C. sporogenes colonizes LLC and CT26 spheroids. *a: experimental setup. b: Intra-spheroid colonization, expressed in colony forming units (CFU)/spheroid (n=3 spheroids per day). Disintegrated spheroids, whereby no bacteria could be detected, are indicated with a triangle. c: Representative images (4x magnification) of LLC (left) and CT26 (right) spheroid overtime treated with control (untreated) or spores (treated). d: Representative fluorescent images of spheroids containing either C. sporogenes-unaG (upper panel) or C. sporogenes-WT (lower panel) in both LLC (day 7) and CT26 (day 9).*

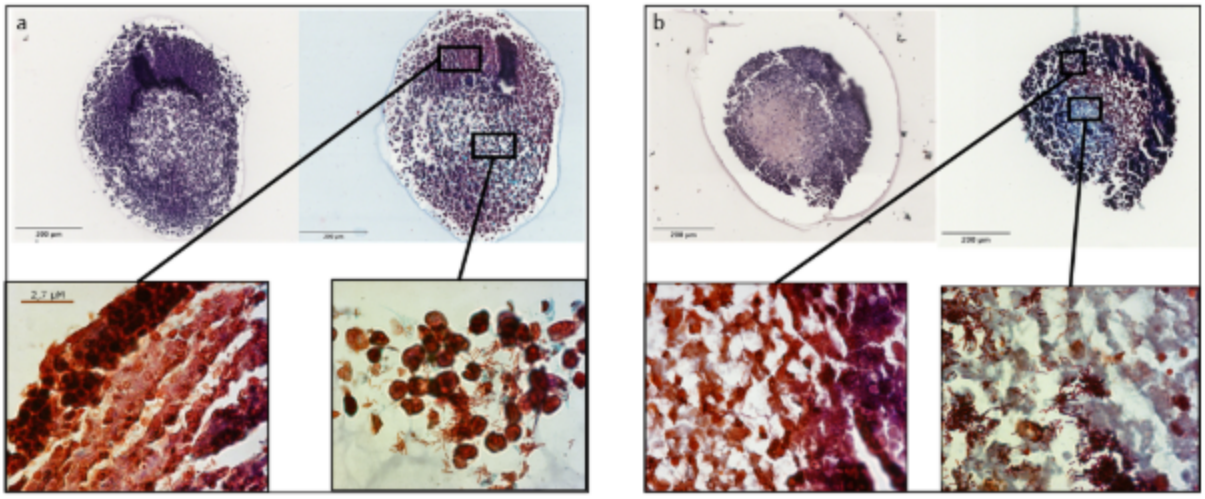


Figure 3

C. sporogenes specifically colonizes the necrotic area of LLC and CT26 spheroids. *Representative images of H&E and gram-staining of LLC (a) and CT26 (b) spheroids, 2 (LLC) and 4 (CT26) days after addition of C. sporogenes spores. For both figures, top panel: H&E staining (left) and gram staining (right), both 4x magnification. Lower panel: zoom into gram staining of the viable (left) and necrotic (right) spheroid area, both 60x magnification (scale bar same for each picture).*

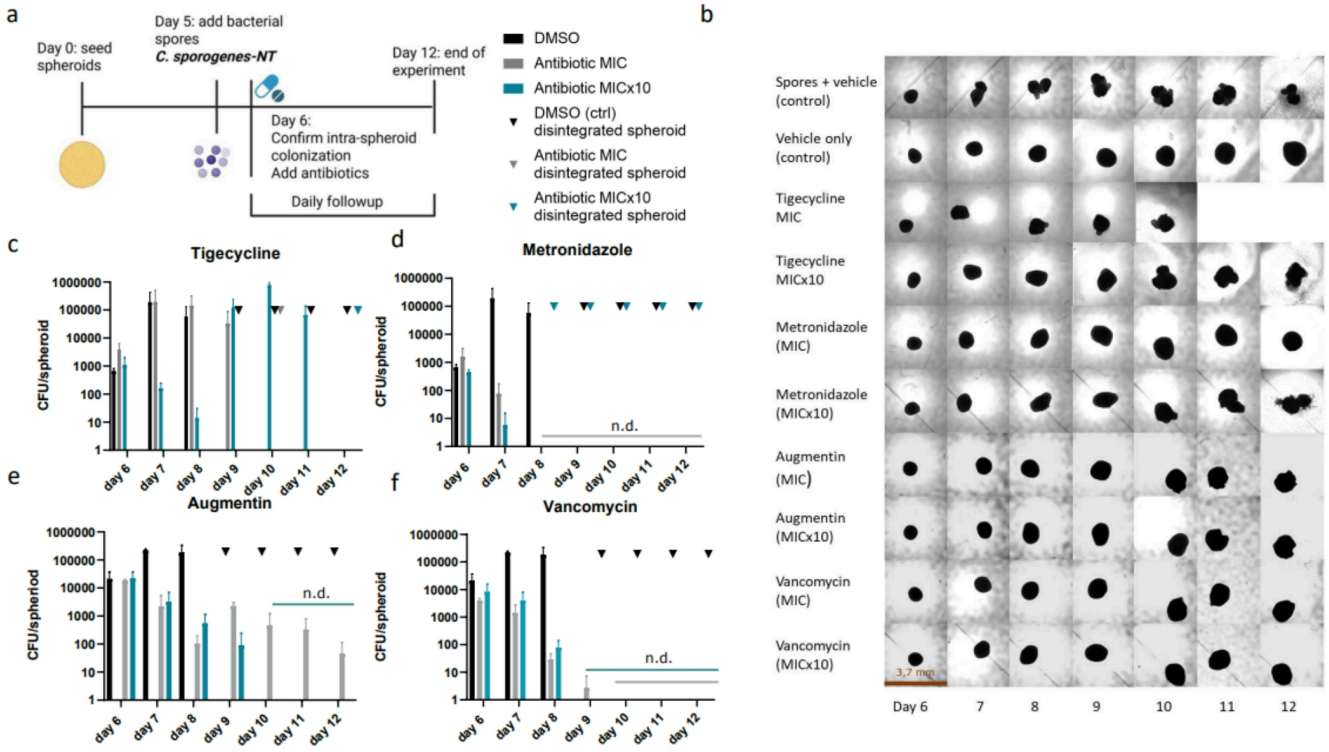


Figure 4

antibiotic clearance of intra-spheroid colonization by C. sporogenes in LLC spheroids. *a: experimental setup. b: Representative images (4x magnification) of LLC spheroids for all treatment groups. c, d, e and f: analysis of intra-spheroid colonization (CFU/spheroid) for each indicated antibiotic (MIC and MICx10). MIC: Minimal Inhibitory Concentration.* n.d.: non detectable.

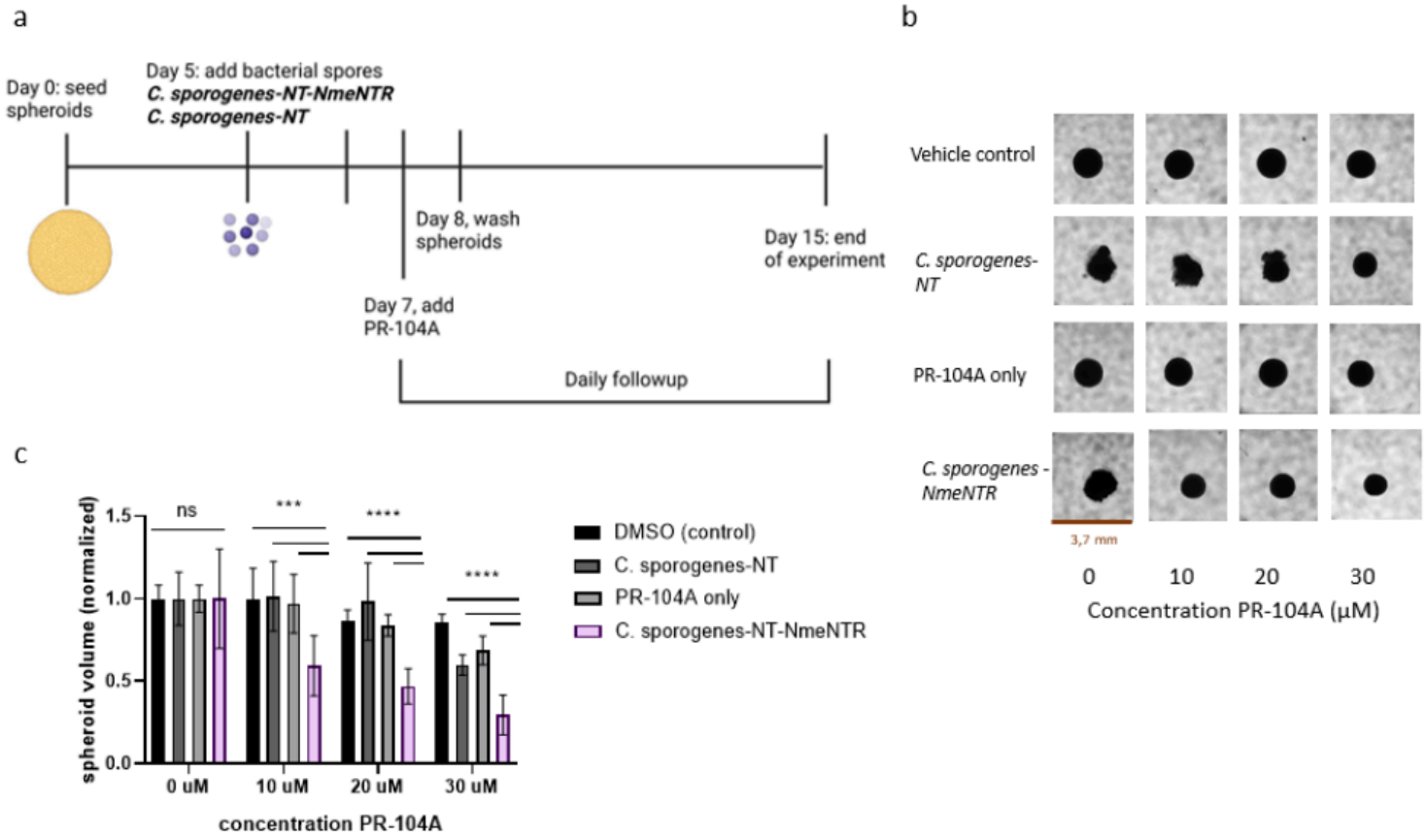


Figure 5

C. sporogenes-NT-NmeNTR combined with PR-104A treatment results in CT26 spheroid growth delay. *a: Experimental setup. b: Representative images (4x magnification) of CT spheroids on day 15 of each experimental group. c: Spheroid volume per experimental group (N=9 technical replicates from 2 biological replicates per group). Y axis: spheroid volume normalized to corresponding DMSO control spheroid volume on day 15. Ns: not significant, P < 0.001 (***), P < 0.0001 (****).*

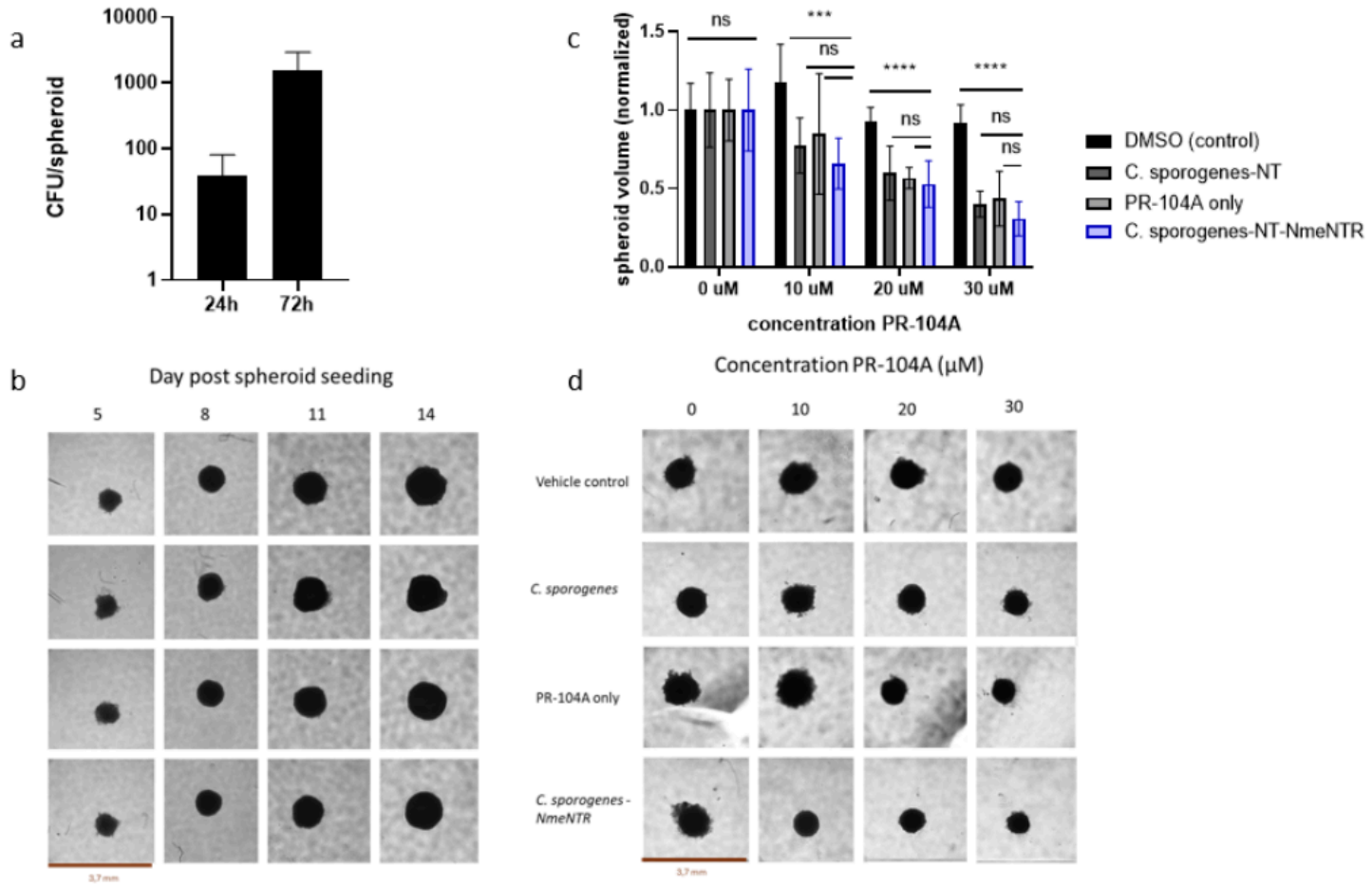


Figure 6

C. sporogenes-NT-NmeNTR combined with PR-104A treatment results in HCT116 spheroid growth delay. *a: CFU/spheroid in HCT116 spheroids 24- and 72-hours post spore treatment (day 5). b: Representative images (4x magnification) of HCT116 spheroids with C. sporogenes-NT intra-spheroid colonization on day 5, 8, 11, and 14 post seeding. c: spheroid volume per experimental group (N=9 technical replicates from 2 biological replicates per group). Y axis: spheroid volume normalized to corresponding DMSO control spheroid volume on day 15. d: Representative images (4x magnification) of HCT116 spheroids on day 15 of each experimental group. Ns: not significant, P < 0.001 (***), P < 0.0001 (****).*

Supplementary Files

This is a list of supplementary files associated with this preprint. Click to download.

- floatimage1.jpeg
- Supplementaryfigures.docx